JOURNAL OF AIRCRAFT
Vol. 31, No. 6, November–December 1994

Analysis of a Higher Harmonic Control Test to Reduce Blade Vortex Interaction Noise

Thomas F. Brooks,* Earl R. Booth Jr.,† and D. Douglas Boyd Jr.‡
NASA Langley Research Center, Hampton, Virginia 23681
Wolf R. Splettstoesser,§ Klaus -J. Schultz,§ and Roland Kube¶
DLR—German Aerospace Research Establishment, Braunschweig D-38108, Germany
Georg H. Niesl**
Eurocopter Deutschland, Munich 81663, Germany
and
Olivier Streby††
Eurocopter France, Marignane 13725, France

A noise study using an aeroelastically scaled BO-105 rotor was conducted in the German-Dutch Wind Tunnel to examine the use of higher harmonic control (HHC) of blade pitch to reduce impulsive blade-vortex interaction (BVI) noise. The noise directivity was measured over a large plane underneath the rotor using a traversing inflow microphone array. Noise and vibration measurements were made for a range of matched rotor operating conditions where prescribed (or open loop) HHC pitch, at various amplitudes and phases, was superimposed on normal (baseline) collective and cyclic trim pitch. Acoustic data are presented for 3, 4, and 5*P* HHC applied to a typical landing approach rotor operating condition where BVI noise is normally intense. Noise reductions of up to 6 dB were found for the advancing side BVI noise radiating upstream of the rotor, and also for the retreating side BVI noise radiating below and downstream of the rotor. The relative levels between the sides were modified by HHC control phase. To help give insight to the physics of the HHC/BVI noise problem, high-resolution loading and noise prediction results are presented for comparison to the data. The predictions are based on a new high-resolution version of the CAMRAD rotor performance program under development at Langley, called HIRES.

Nomenclature

a_0 = speed of sound in air, m/s
C_T = rotor thrust coefficient, thrust/$\rho\pi R^2(\Omega R)^2$
f = frequency, cycles/s
f_{bp} = blade passage frequency, number of blades × $\Omega/2\pi$
L = blade lift, N
M_T = hover tip Mach number, $\Omega R/a_0$
nP = nth harmonic of rotor rotational period
P = per revolution
R = rotor radius, m
x = streamwise coordinate relative to hub, m
y = crossflow coordinate relative to hub, positive on advancing side, m
z = vertical crossflow coordinate relative to hub, m
α = rotor tip path plane angle referenced to tunnel streamwise axis, deg
α' = effective α corrected for open-jet wind-tunnel effect, deg
Γ = tip vortex strength, m²/s
Θ = calculated full-scale flight descent angle, positive in descent, deg
θ = pitch angle of blade at Ψ, deg
θ_c = amplitude of higher harmonic pitch at Ψ_c, deg
μ = advance ratio, tunnel flow velocity/ΩR
ρ = density of test medium, kg/m³
σ = rotor solidity
ϕ = HHC system phase angle, pitch amplitude, $|\theta_c|\cos(n\Psi - \phi)$
Ψ = blade azimuth angle, deg
Ψ_c = blade azimuth angle corresponding to θ_c, deg
Ω = rotor rotational speed, rad/s

Introduction

IMPULSIVE blade-vortex interaction (BVI) noise is one of the most objectionable types of helicopter noise. This midfrequency noise is particularly evident and generally dominant during low-speed descent flight, as in a landing approach and during maneuvers. The noise is due to blades interacting with the shed tip vortices from the preceding blades. Reductions in tip vortex strength, increases in blade-vortex separation distances, or reduction of blade pitch during BVI can be expected to reduce the intensity of the BVI fluctuation loading and, thus, noise.[1] All of these parameters are addressable through the use of higher harmonic control (HHC) of blade pitch angle, which has historically been used for vibration reduction.[2] An illustration of HHC usage for noise reduction on a rotor is given in Fig. 1. Changes in pitch modify the tip vortex strengths, as well as their trajectories and subsequent blade encounter.

Two independent wind-tunnel studies, conducted in the same time frame, of the use of HHC to reduce BVI noise have been reported. One of the tests, conducted in NASA Langley's Transonic Dynamics Tunnel (TDT) and reported by Brooks et al.,[3,4] examined the use of 4*P* HHC pitch at various amplitudes and phases. The scheduled (or open loop) controls were superimposed on the normal collective and 1*P*

Received Dec. 5, 1991; revision received Nov. 15, 1993; accepted for publication March 15, 1994.

*Senior Research Scientist, Acoustics Division. Senior Member AIAA.
†Research Engineer, Acoustics Division.
‡Research Engineer, Lockheed Engineering and Sciences Co.
§Senior Research Scientist, Technical Acoustics Division, Institute for Design Aerodynamics.
¶Research Scientist, Institute of Flight Mechanics.
**Development Engineer, Aerodynamics and Acoustics Branch.
††Research Engineer, DE CAB.

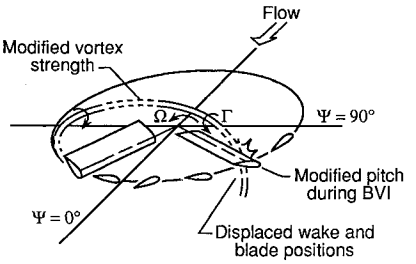

Fig. 1 Illustration of HHC noise reduction concept.

cyclic trim pitches for a large number of simulated rotor flight conditions. The rotor tested was a dynamically scaled Sikorsky H34 with fully articulated flap and lead-lag hinges. Midfrequency noise reductions of up to 5 or 6 dB were found for low-speed descent conditions. However, low-frequency loading noise was found to increase, along with some increase in vibration level. The other test mentioned was conducted in the closed test section in the German-Dutch Wind Tunnel (DNW).[5] The hingeless rotor was a dynamically scaled BO-105 rotor. This test found similar BVI noise reduction to that of the TDT study. Three HHC controls (3, 4, and 5*P*) were tested and produced similar noise reductions and vibration levels. Significant BVI noise reductions were also found in open and closed (iterative) loop HHC noise and vibration control flight testing on a Gazelle helicopter.[6]

A severe limitation on the previous wind-tunnel and flight tests was the lack of directivity information. The TDT test employed sound power measurement methods in a hard wall closed tunnel, and the closed test section DNW test used a limited number of microphone positions in a reflective environment. Recognizing that noise directivity is required to establish the noise reduction potential of HHC, a three-nation cooperative test program was undertaken. The present study obtained detailed noise directivity and vibration measurements of a scaled rotor, undergoing HHC, in the quality acoustic environment of the DNW open test section. Open loop 3, 4, and 5*P* HHC, as well as some mixed 3*P*/4*P*/5*P* HHC modes, were tested over a range of rotor operating conditions. Splettstoesser et al.[7] document the test and its results in some detail, and address a number of issues raised in the previous studies. This article deals with a subset of the midfrequency noise data. The data provide a focus for an analysis of the physics of the effect of HHC on BVI noise and serve to partially validate a prediction approach.

Test Program

As detailed in Ref. 7, the test was conducted in the open anechoic test section of the DNW. Figure 2 shows the DLR model rotor test stand mounted on the DNW sting, along with the traversing inflow microphone array that is situated underneath. The four-bladed hingeless rotor is a 40%, dynamically scaled model of a MBB BO-105 main rotor. The 4-m-diam rotor has 121-mm chord, NACA 23012 section blades with an 8-deg linear twist and a standard rectangular tip.

The inflow microphone array is comprised of 11 microphones spaced 0.54 m apart on a horizontal wing. The array is traversed 4 m forward and 4 m aft of the rotor hub in the x direction. As illustrated in Fig. 3, this creates a large 5.4- by 8-m measurement plane, 2.4 m underneath the rotor. Thirty rotor revolutions of microphone data, at 1024 samples/revolution, were taken at each streamwise step, 0.5 m apart. Bandpass filtering was used to limit the data to the frequency range from 40 Hz to 9 kHz.

Pitch control is applied to the rotor through swashplate motions due to three electrohydraulic actuators. Conventional collective and 1*P* cyclic trim pitches are attained by mean positioning of the actuators. The higher harmonic pitches of 3, 4, and 5*P* are attained separately or in combination for the four-bladed rotor by proper phasing of 4*P* input to the actuators.[8]

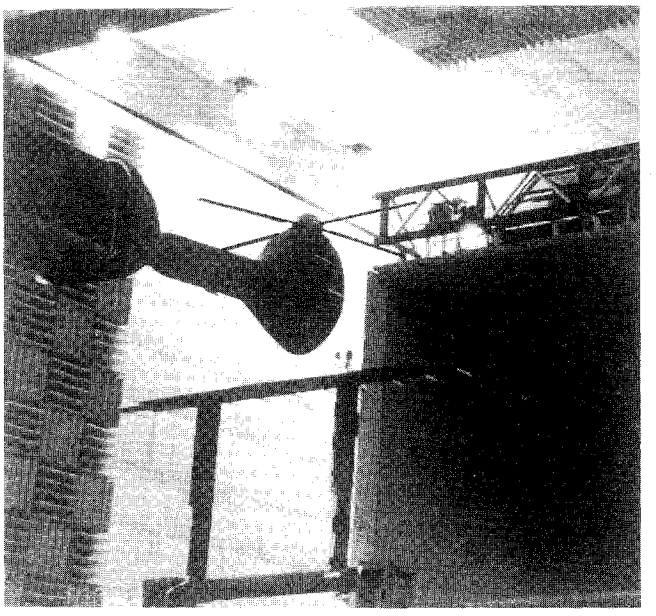

Fig. 2 DLR rotor model and microphone traverse in the DNW open test section.

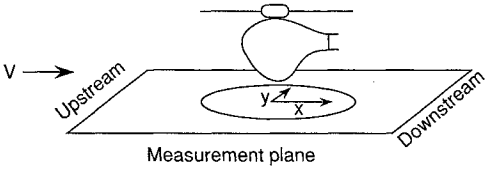

Fig. 3 Noise measurement plane under rotor, as mapped out by traversing microphone array.

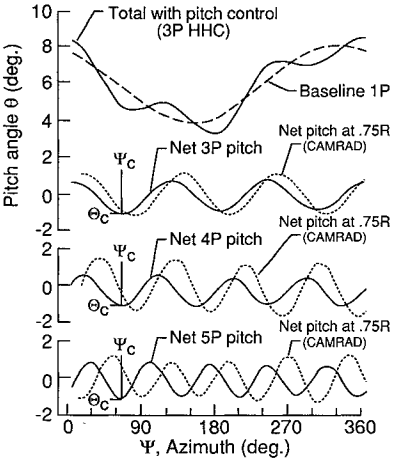

Fig. 4 θ vs Ψ_{HHC} for $\mu = 0.15$ and $\alpha' = 3.8$ deg ($\Theta = 6$ deg). Pitch control is 3, 4, and 5*P* at $\theta_c = -0.8$ deg and $\Psi_c \approx 60$ deg.

To illustrate how pitch was controlled in the test, Fig. 4 shows blade pitch measured at the blade root as a function of blade azimuth for a specific simulated flight condition. The baseline (no HHC) case is seen to require a 6.0-deg mean collective, and a 2.1-deg 1*P* cyclic pitch for thrust and zero-moment (zero-flapping) trim, respectively. For the HHC test cases, 3, 4, or 5*P* pitch schedules are superimposed (3*P* is shown) on the baseline condition. When applying HHC for this test, little or no adjustments were found necessary in mean collective and cyclic to maintain trust and trim conditions. In Fig. 4, the difference between the total and baseline pitch schedules shows the net HHC pitch for the 3*P* case, as well as the different 4*P* and 5*P* cases. For this report, the HHC conditions are specified in terms of negative peak HHC θ_c, in the first rotor quadrant region, at Ψ_c. For 3*P*, 0 deg $\leq$

$\Psi_c < 120$ deg; for 4P, 0 deg $\leq \Psi_c < 90$ deg; and for 5P, 0 deg $\leq \Psi_c < 72$ deg. The DLR control system phase ϕ is also noted for reference. In Fig. 4, each of the 3, 4, and 5P cases have $\theta_c = -0.8$ deg at $\Psi_c \approx 60$ deg. Also shown in Fig. 4 are predictions for net HHC pitch at 75% blade radius based on CAMRAD performance calculations to be discussed. The observed offset in pitch amplitudes and phases compared to the measured blade root values result from blade torsional aeroelasticity effects.

The rotor was tested over a range of simulated low-to-moderate descent flight conditions. $\Omega = 1050$ rpm (the nominal $M_T = 0.64$), giving $f_{bp} = 70$ Hz. C_T was maintained at 0.0044, giving $C_T/\sigma = 0.057$. α were corrected[9] to account for open wind-tunnel effects to obtain equivalent freestream (or corrected) α' values. Also, Θ were calculated[9] based on fuselage-rotor drag of a MBB BO-105.

Test Results

In this section, acoustic results are presented to illustrate the effects of HHC on rotor noise characteristics. Emphasized is a particular low-speed descent condition where 3, 4, and 5P HHC at different amplitudes and phases are employed. The results provide a comparison for BVI noise analysis of the HHC problem. Reference 7 includes a more complete data base.

Directivity and Waveform Characteristics

The effect of HHC on rotor noise is shown in Fig. 5 for a typical landing approach condition of $\Theta = 6$ deg, at a speed corresponding to $\mu = 0.15$. The directivities of BVI noise and sound pressure time histories are shown for the baseline (no HHC) case and two 4P HHC cases for $\theta_c = -0.8$ deg, where $\Psi_c = 1$ deg ($\approx$0 deg), and 61 deg ($\approx$60 deg). The directivity mappings of Fig. 5a are for the midfrequency noise levels. These levels are obtained from the noise spectra by integrating from the 6–40 blade passage harmonic. This midfrequency level is dominated by BVI noise contributions in the descent test cases of the present study and, because of frequency and level, has been found to follow closely the subjective noise measures of weighted sound pressure level (dBA) and perceived noise level (PNL) for equivalent full-scale flight conditions.

The baseline directivity plot in Fig. 5a is consistent with previous studies (e.g., see Ref. 10), and shows two distinct BVI noise directivity lobes defined by the higher level regions (shaded in the figure). One lobe is directed forward and to the side of the rotor, due to advancing side BVI occurrences, and another is directed aft of the rotor, due to retreating side BVI. The use of 4P HHC at 0.8-deg amplitude is seen to significantly modify the directivity levels. For $\Psi_c = 1$ deg, the advancing side BVI peak levels are reduced by 3 dB, whereas those of the retreating side are reduced by 5 dB. For $\Psi_c = 61$ deg, the advancing side BVI noise level is reduced by 2 dB, but that of the retreating side is increased by almost 3 dB. Away from the directional lobes, there is some increase in levels with the use of HHC.

The acoustic pressure time histories shown in Fig. 5b, for the corresponding conditions of Fig. 5a, were obtained by averaging data from 30 rotor revolutions. Microphone positions at $(x, y) = (0.0$ m, 2.16 m) and (2.0 m, -1.08 m) represent intense advancing and retreating side BVI noise locations, respectively. For the baseline case, the pressures of the two sides are seen to have different impulsive characteristics (apparently of opposite polarity), but both are of BVI origin. It is noted that even microphone positions within the same BVI noise directional lobe can have somewhat dif-

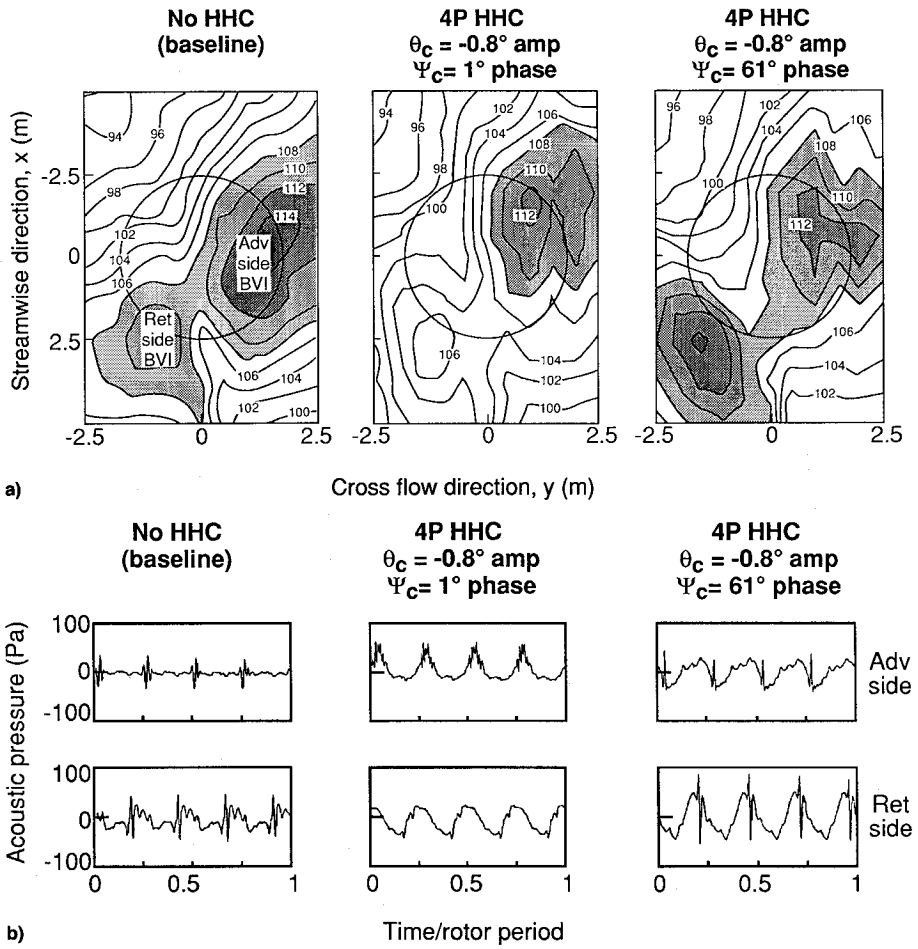

Fig. 5 Directivity and acoustic signatures for baseline and two HHC applications for $\mu = 0.15$ and $\Theta = 6$ deg: a) midfrequency (BVI) noise directivity over measurement plane and b) microphone time histories on advancing and retreating sides.

ferent waveform shapes.[10] For Ψ_c = 1 deg HHC pressure histories, the advancing side shows evidence of multiple occurrences of BVI, although with lower impulsive amplitude levels. For the retreating side, the impulsive noise is substantially reduced. At Ψ_c = 61 deg, the impulsive characteristics change some for both sides, with amplitudes changing little for the advancing side, but increasing for the retreating side.

A significant feature of the pressure histories for 4*P* HHC is the increase in low-frequency noise, primarily at the blade passage frequency. The increase is due to the resultant higher harmonic loading. It has been found that the low-frequency noise increase is somewhat less for 3*P*, 5*P*, and combination 3*P*/4*P*/5*P* HHC. This low-frequency level increase would, of course, be considered a matter for concern for any actual application of HHC for helicopters. It should be noted, however, that the measurement plane is in the acoustic near field with respect to the low-frequency noise, but far field for the individual BVI noise sources. This tends to overemphasize the low-frequency contribution and its relative importance. Also, with regard to subjective dBA or PNL measures, the low-frequency increases contribute very little. Still, low-frequency noise increases are not desirable, so blade pitch motion that does not reduce BVI noise should be minimized in any practical applications.

Figure 6 shows how midfrequency (BVI) noise directivity is affected by the use of different θ_c amplitudes and Ψ_c phases of 4*P* HHC. The contour presentations are similar to Fig. 5a, but with the lower level contour lines and labeling removed. The baseline directivity and contour shading region are shown in Fig. 6a. The considerable influence of phase on BVI directivity and level is seen in Fig. 6b for the amplitude θ_c = −0.8 deg. The contours suggest substantial modification of the BVI occurrences with reduction or elimination of certain interactions and the increase or commencement of others. The Ψ_c = 1- and 61-deg cases, also shown in Fig. 5, have the lowest levels. Increasing the pitch amplitudes from θ_c = −0.8 to −1.2 deg, as shown in Fig. 6c for the same 4*P* HHC, does not appear to significantly alter the directivity, but can amplify increases or decreases in level for corresponding control angles. A case not shown in Fig. 6c, because of the even phase spacing, is for Ψ_c = 54 deg, where the advancing side BVI noise levels were reduced 6 dB. Reference 7 shows this and the directivities obtained when using 3 and 5*P* HHC. These controls produced similar directivity behaviors, compared to 4*P* HHC, but at different phases.

Figure 7 is presented to show the effect of HHC control mode and phase on noise levels. Figure 7a shows the change, ΔdB, in the maximum measured advancing and retreating side BVI noise levels compared to baseline levels, with the use of 3*P* HHC at θ_c = −0.8. The data are presented as a function of control phase Ψ_c. Figures 7b and 7c show ΔdB levels with the use of 4 and 5*P* HHC for θ_c = −0.8 deg. The square symbols represent HIRES predictions, discussed below. The presentations of the measured data demonstrate a cyclic, although not generally sinusoidal, behavior of the BVI noise level change with control phase.

Operational Variations

The effects of the use of a specific HHC application on midfrequency noise levels are given in Fig. 8 for a range of simulated flight conditions. The contour levels in Figs. 8a and 8b are determined by mean-square-pressure-averaging over the measurement plane for the baseline and 4*P* HHC cases. The operating conditions are defined by Θ and μ. As seen on the plots, the number of grid or test points defining the contours are limited, especially at the lowest μ value. However, confidence in the contour details is aided by their great similarities to sound power level plots of Ref. 3 for the TDT test.

The most intense baseline BVI noise (Fig. 8a) is seen to be at lower speeds in a curved band that increases with Θ as μ is reduced. The "typical" Θ = 6.0 deg and μ = 0.15 descent

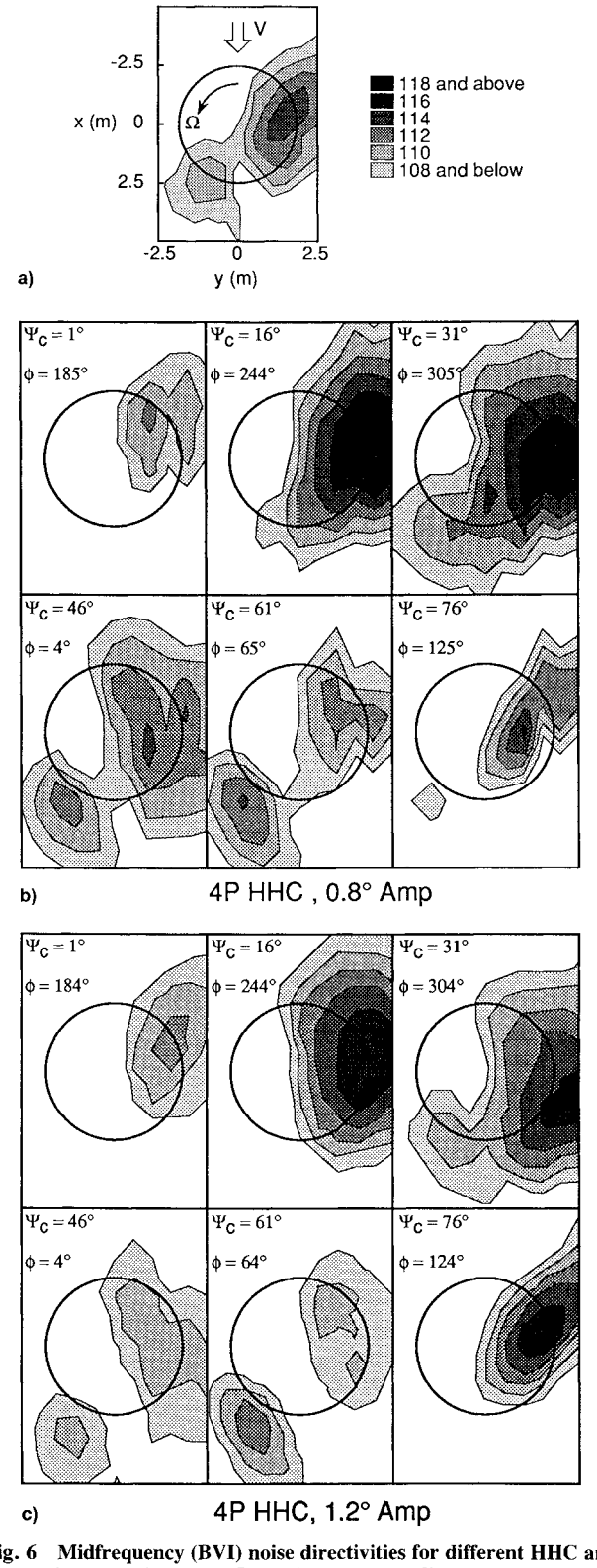

Fig. 6 Midfrequency (BVI) noise directivities for different HHC and phases for μ = 0.15 and Θ = 6 deg: a) baseline, no HHC, b) 4*P* HHC, θ_c = −0.8 deg, and c) 4*P* HHC, θ_c = −1.2 deg.

condition of concern in this report is within 1.0 deg of descent, or alternately 1.0 dB, of the maximum BVI condition at μ = 0.15. The dashed line, designated as Θ_{BVI}, indicates the condition where the rotor is operating in its own wake, calculated using the method described in Ref. 11.

For comparison to the baseline levels of Fig. 8a, Fig. 8b shows noise levels found when 4*P* HHC at Ψ_c = 1 deg and θ_c = −0.8 deg was employed over the operating range. A contour showing the difference or change in levels between the baseline and HHC conditions is shown in Fig. 8c. The

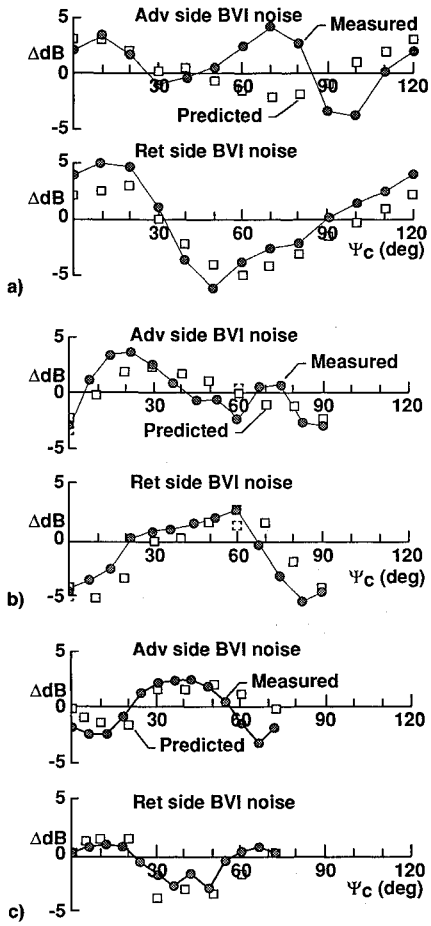

Fig. 7 Change in maximum advancing and retreating side BVI noise level (ΔdB = dB_{HHC} − $dB_{No\,HHC}$) vs HHC phase for μ = 0.15 and Θ = 6 deg: a) 3*P*, b) 4*P*, and c) 5*P*, HHC, θ_c = −0.8 deg.

negative levels represent noise reduction using HHC and positive levels represent increase. It is seen up to 4–5-dB reduction can be found for this particular (nonoptimum) control over certain operating conditions. It should be emphasized that Fig. 8c does not represent the full potential of HHC noise reduction. If optimum HHC conditions were found at each operational point, Fig. 8c would show significant noise reductions over much larger ranges. Examples of this are shown in Ref. 7. The present result does correctly indicate, however, that HHC is most useful at low-speed descent conditions where BVI noise is most intense.

Comparison with Results for Different Rotor

The NASA TDT test[3,4] showed noise reductions, using HHC, comparable in magnitude to the current test, but the required control input amplitudes and phases differed. It appears that rotor aeroelasticity has an important role in the BVI noise results. The present rotor is hingeless with linearly twisted dynamically scaled BO-105 blades. The first torsional mode is calculated in CAMRAD[12] to be 3.9 per revolution (3.9*P*). This is torsionally soft and results in calculated pitch amplifications that are shown in Fig. 4. For the TDT test, the dynamically scaled Sikorsky H34 rotor was fully articulated with relatively stiff, untwisted blades. The first torsional mode calculated for the rotor is 9.1*P*, which gives only about a 10% pitch amplification at 0.75*R*, and a 3- to 4-deg lag for the 4*P* control tested.

As mentioned for Fig. 8, the noise level dependence on rotor operating conditions with and without the use of 4*P* HHC is similar to the TDT results. The differences found, however, include a shift in descent angle of 1.5 deg required to define the maximum BVI noise condition. Also of significance, the control phase dependences are different between

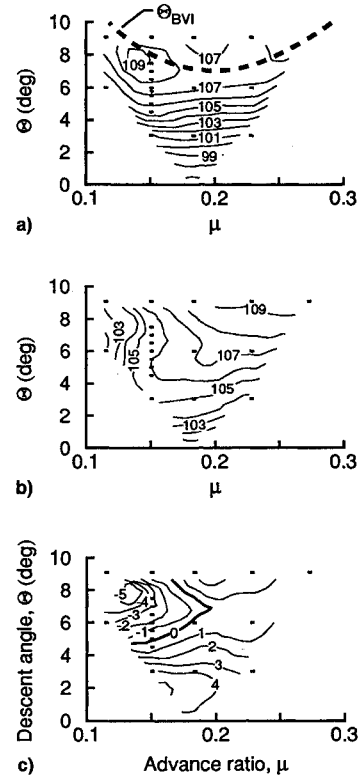

Fig. 8 Effect of HHC on spatially-averaged midfrequency (BVI) noise levels as a function flight condition: a) baseline (no HHC), b) 4*P* HHC at $\Psi_c \approx$ 60 deg and $\theta_c \approx -0.8$ deg, and c) difference, ΔdB = dB_{HHC} − $dB_{No\,HHC}$.

the two rotors. $\Psi_c \approx 0$ deg for the present data, and $\Psi_c \approx 60$ deg for the TDT data produced the greatest noise reduction. The present study then serves to undercut an implication in Ref. 3 that maximum BVI noise reduction corresponds to minimum local pitch at BVI locations (assumed to be in the vicinity of 60 deg).

Interestingly, for low-frequency noise, comparing the results from Refs. 3 and 7, one finds the levels to have the same Ψ_c dependence if the 20-deg lag in outboard pitching of the DLR blades is taken into account. This is what one would expect theoretically since the cyclic loading (the cause of low-frequency noise) is more concentrated in the outboard portion of the blades. Another important comparison is for vibration loading, which appears to have similar Ψ_c dependences, even without the 20-deg lag being taken into account. These differences in functional behaviors with Ψ_c points out the lack of a one-to-one causal relationship between the reduction or increase in midfrequency (BVI) noise, low-frequency noise, and vibration.

Analysis

The instrumentation of the blades included only inboard strain gauges and no surface pressure measurements. In order to understand the mechanisms of noise generation, with and without the use of HHC, an analytical approach for the determination of important aeroelastic and aerodynamic features was developed.

High-Resolution Load Calculations

The basis for the present analysis is a high-resolution version of CAMRAD, called HIRES. CAMRAD[12] is a rotor performance code that employs free wake and blade dynamics models that permit calculation of blade twisting and flapping motion, as well as free tip vortex wake trajectories. The loading calculations for CAMRAD are based on lifting line theory that models the unsteady aerodynamics, including compressibility effects and stall.

The approach taken in the development of HIRES was to first increase the resolution of CAMRAD to the intrinsic practical limit (found to be 10-deg azimuth). The capability of HHC was incorporated into the code. Postprocessing codes were then developed to determine blade positions and wake (tip vortices) strength and trajectories at very small incremented steps. At each step, the induced velocities and blade sectional loadings are calculated from the rotor's bound vorticity, tip vortices, and inboard wake vorticity, plus the "flight" velocity contribution. At the time of this article, the inboard wake modeling in the near wake is not high resolution. This lack of localized three-dimensional near-wake shedding influence tends to cause the unsteady load amplitudes to be somewhat overpredicted, more so for skewed gust encounters than for parallel (two-dimensional) encounters. However, this limitation is of little or no consequence here because of the way the analysis is used.

Applications of HIRES are shown in Fig. 9 for the same baseline and HHC conditions of Fig. 5. The CAMRAD code is run in a normal fashion and trimmed to the nominal rotor and tunnel conditions of C_T, μ, and α' for zero flapping (~zero moment). The tip vortex core radius employed was $0.03R$, which is likely larger than actual viscous core radii, but is in line with that proposed by Johnson[13] to attain proper trim. In CAMRAD, the core radius size parameter represents not only the actual size, but also all phenomena of the blade-vortex interactions that are not otherwise modeled.

The contour plots of Fig. 9a show rotor disk loading, which is the lift encountered by the blades as they rotate. The resolution shown is 1.0-deg azimuthally at 75 radial stations. The areas or lines of intense loading reveal where the blades encounter the tip vortices. Comparisons are made in Fig. 9b of the spanwise integrated load (lift) as a function of blade azimuth at 1-deg resolution compared to the full-CAMRAD results at 10-deg resolution. CAMRAD is seen to miss the BVI occurrences entirely. The effect of HHC on the aerodynamics is significant. The $4P$ cyclic loading is seen to be superimposed on the disk loading in a nonlinear way. Part of this behavior is due to torsional blade twisting that results in azimuthal phase lags in pitch of the outboard portions of the blades. This was discussed in the last section and shown in Fig. 4. For the $4P$ case, corresponding to the Ψ_c = 61-deg case of Fig. 9, the lag is about 20-deg azimuth.

Acoustic Analysis Using Calculated Loads

For the BVI noise problem, the most important features are those related to the intensity and geometry of the BVI occurrences. In the second and third rotor quadrants (from Ψ = 90 to 180 deg and from 180 to 270 deg, respectively), the blades are seen in the contours of Fig. 9a to encounter the tip vortices, which are above the blades, at highly skewed angles. At high skew angles, the interaction loads skim across the span of the blades at subsonic (phase) speeds and, thus, do not radiate impulsive noise efficiently to the far field.[14] At less skewed angles, such as those found in the first and fourth quadrants (from Ψ = 0 to 90 deg and from Ψ = 270 to 360 deg, respectively), where the phase speeds are often sonic or higher, impulsive noise is radiated. The most efficient radiation is found where blades interact with the vortices at near parallel angles, giving a principal radiation that is normal to the blades. A near parallel interaction is seen to occur for the baseline contour near Ψ = 60 deg. The Ψ = 60-deg blade position is indicated in Fig. 9a. Here, the locally intense interaction region over the inboard section for the blade is where the blades intersect tip vortices as they cross from above to below the rotor disk. A number of these crossover interactions are seen to occur downstream between Ψ = 60 and 0 deg. Another near parallel interaction is also seen to occur at about Ψ = 300 deg in the outboard region near the tip. The corresponding lift vs azimuth plot in Fig. 9b shows both the Ψ = 60- and 300-deg regions to have substantial net lift fluctuation within short azimuthal increments. The contour

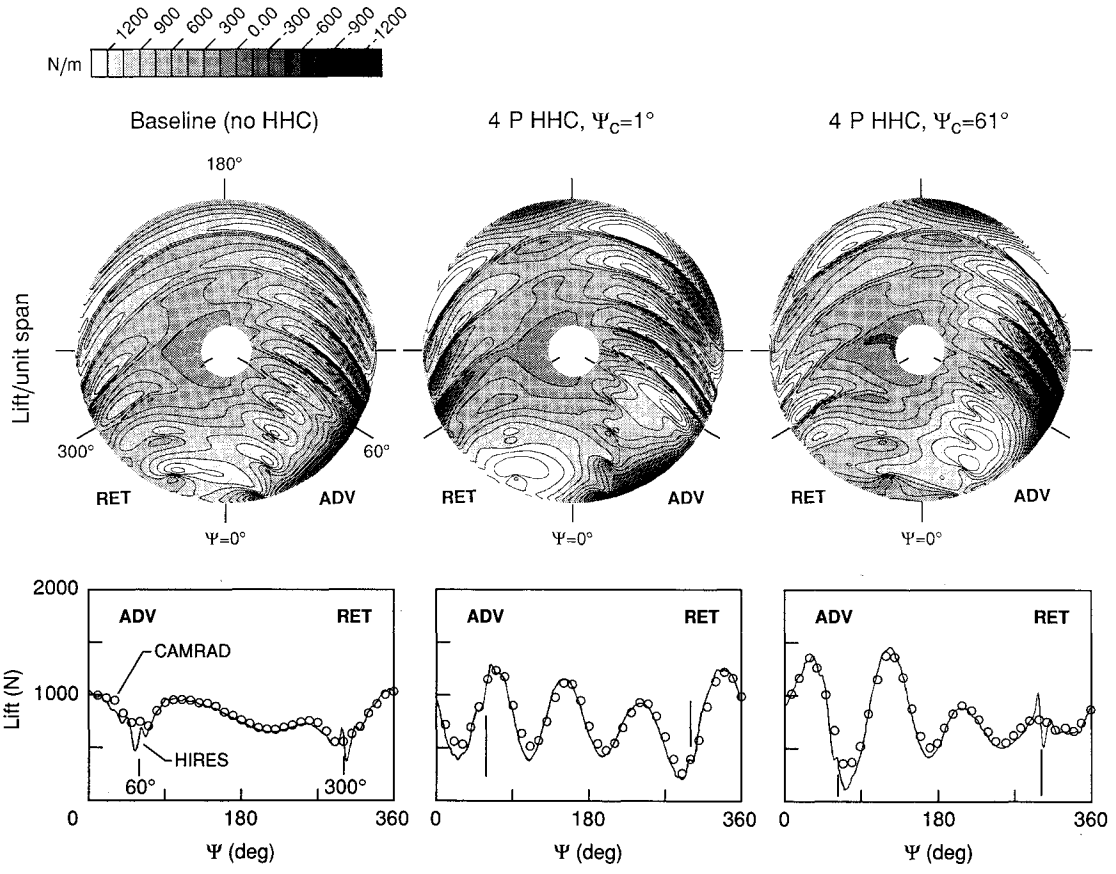

Fig. 9 High resolution disk loading calculations using HIRES for the baseline and HHC case of Fig. 5: a) loading distribution contours and b) total blade lift vs azimuth.

for the 4P HHC/Ψ_c = 1-deg case shows some disruption (or smoothing out) of the sharply defined BVI loading fluctuation at Ψ = 60 and 300 deg, compared to the baseline case. This is also true to some extent for the 4P HHC/Ψ_c = 61-deg case at Ψ = 60 deg, but for Ψ = 300 deg the fluctuation is stronger.

The qualitative discussion of Fig. 9 can be made quantitative by the presentation in Fig. 10. The contour plots are of the azimuth derivative of blade loading, d(L/span)/dΨ (actually here dΨ = $\Delta\Psi$ = 1 deg). The contour plots can be thought of as representing potential noise source strength distributions, because the noise radiated is proportional to the time derivatives dt of loads, and dΨ = Ω dt. As mentioned, the BVI skew angles determine the radiation directions. The noise radiated to an observer directly under the rotor in the far field can be obtained by a simple spanwise integration of the loading derivatives, since there are no retarded time delay differences over the rotor for this observer. This is shown in Fig. 10b and represents the acoustic pressure time history behavior predicted for one blade in one revolution. To allow easy comparison to the related measured results of Fig. 5b, dL/dΨ is expressed in terms of acoustic pressure Pa units obtained by modeling the rotor simply as an acoustic dipole[15] for an observer distance of r = 2.4 m. That plotted is actually $p'(\Psi) = (\Omega/4\pi a_0 r)(dL/d\Psi)$. By comparing these calculated results with Fig. 5b for the baseline case, the similarity in waveform (or pulse shapes), as well as separate acoustic time delay calculations, indicate that the Ψ = 60- and 300-deg blade positions are associated with the most positive and most negative measured acoustic pulses on the advancing and retreating sides, respectively. Corresponding comparisons for the HHC cases find, again, many similarities in the waveform shape and amplitude behavior for the respective sides.

The $p'(\Psi)$ term of Fig. 10b is the predicted noise signature of a rotor blade, modeled as a simple compact acoustic dipole. As such, it can be used as a predictor of the effect of HHC on advancing and retreating side BVI noise. To allow comparison with the measured midfrequency noise level results, $p'(\Psi)$ is first filtered to remove low-frequency contributions. For the advancing side, a decibel (dB) level is determined as 10 $\log_{10}$ of the mean-square-value of the filtered $p'(\Psi)$ between Ψ = 0 and 90 deg. For the retreating side, the same is done between Ψ = 270 and 360 deg. Differences in calculated levels between HHC and baseline conditions, $dB_{HHC} - dB_{NoHHC}$, represent the reduction or increase in levels ΔdB with the use of HHC.

In Fig. 7, the calculated ΔdB levels are compared to the measured values for the 3, 4, and 5P control modes at an amplitude of θ_c = −0.8 deg over the full range of azimuth control angles Ψ_c. For the 3P HHC case of Fig. 7a, good level and trend agreement is seen for the retreating side. In Fig. 7b for 4P, generally good agreement is found, such as for the Ψ_c = 1- and 61-deg cases, which are studied in some detail in this article. For the 5P case of Fig. 7c, even better overall agreement is found.

Importance of Key Parameters

Figure 11 shows the predicted geometry of the blades and the closest tip vortex at the instant of time where Ψ = 60 deg for the baseline, as well as for the two 4P HHC cases. Also, the BVI geometry for the blade is shown at a different time where the position is Ψ = 300 deg. The top or plan view of Fig. 11a, which matches the x, y coordinate system of Fig. 3, shows there are only small differences in the lateral or longitudinal vortex positions with the use of HHC. However, as seen in Fig. 11b for elevation z (rotor hub at z = 0), significant changes in vortex-blade separation or "miss" distances and crossover geometries are found. For 4P HHC/Ψ_c = 1 deg, the vortex crossing at Ψ = 60 deg is more inboard than that of the baseline, and the mean vortex-blade separation distance in this region is larger, due to a steeper vortex crossover angle. Evidence of this crossover geometry change is also seen in Fig. 10a for the Ψ = 60-deg position and other interactions downstream on the rotor disk. These changes should and do reduce the BVI noise.

It is noted that cyclic blade flapping due to the use of HHC is likely to be of little consequence to the BVI problem. The

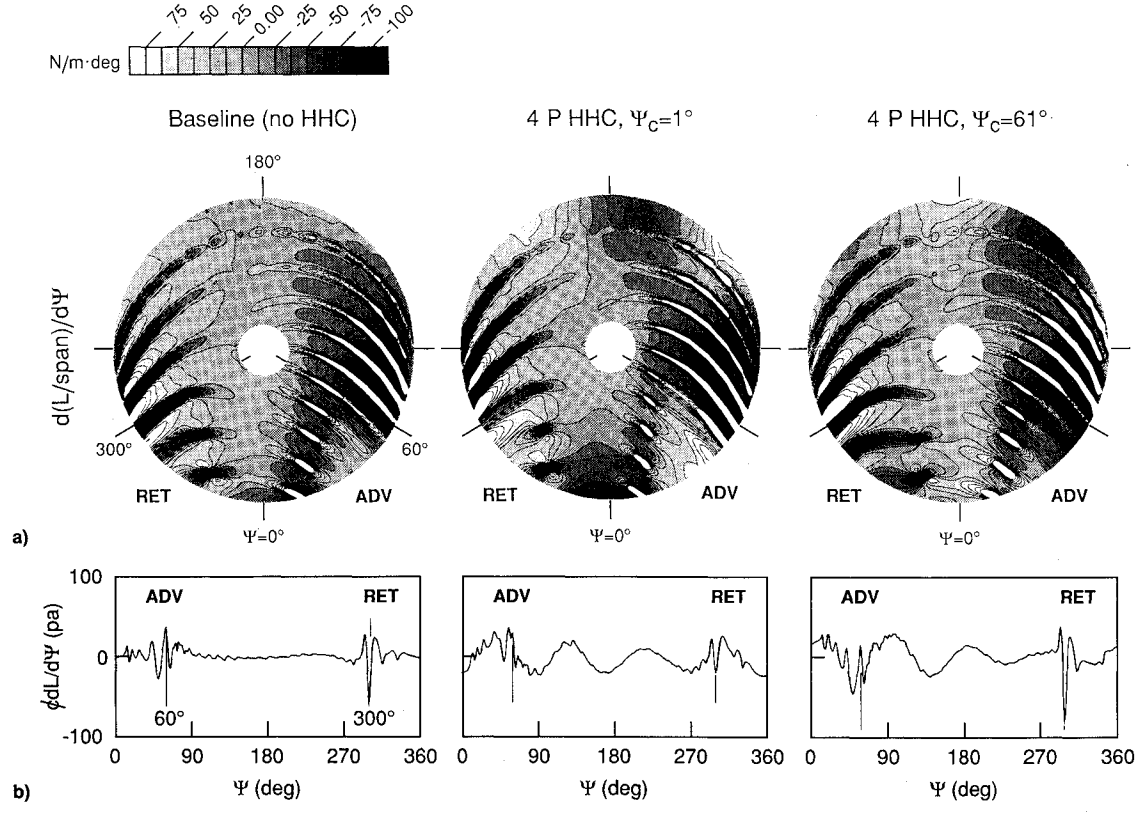

Fig. 10 Rate of change of blade loading with azimuth angle for cases of Fig. 9: a) rate of change distribution contours and b) rate of change of total lift vs azimuth. The term ϕ = $(\Omega/4\pi a_0 r)$.

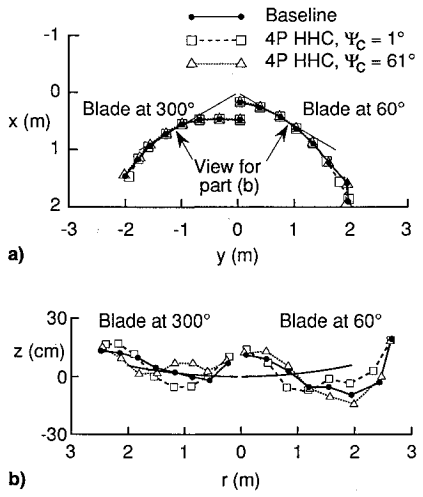

Fig. 11 Geometry of blade and tip vortices for the BVIs occurring at Ψ = 60 deg, and later at Ψ = 300 deg for the baseline and HHC cases of Fig. 9: a) top or plan view and b) views from behind and normal to blade at Ψ = 60 and 300 deg.

calculations show only small flapping deflection (less than ±1 cm at the tip for $\theta_c = -0.8$ deg) compared to the tip vortex offset distances. The position of a vortex element is due to the integrated effect of the induced velocity acting along its path over the rotor disk, after being initially shed from a blade tip upstream in the second or third quadrant. This is important because it means that the global cyclic-lifting effects on the rotor disk, discussed for the 4*P* HHC usage in Fig. 9, determine the vortex trajectory and, thus, the BVI geometry. This connection between global and localized effects, of course, has ramifications for defining successful HHC modes.

The calculations incorporate Γ variations due to the higher harmonic loading. In CAMRAD, the strength of a vortex segment is modeled as being equal to the maximum bound circulation on the blade at the blade position where the vortex was shed from the tip. Evidence of HHC cyclic variations in strengths can be seen at interactions downstream of high and low blade loading in Fig. 9a. Some special HIRES calculations were made to isolate the importance of this parameter. Figure 7b has several ΔdB-predictions, shown by the dashed square symbols, for which the vortex strengths were forced to equal those of the baseline. It is seen that, with everything else being equal, Γ produced predicted level changes from 0.5 to 1.5 dB. Of course, the effects are not actually separable as the vortex strengths help to define the vortex trajectories.

An effect not modeled in the aerodynamics of CAMRAD or any other commonly used unsteady aerodynamics modeling is the influence of mean blade loading on the intensity of gust or BVI blade response. A number of studies by Kerschen et al.,[16–18] as well as that of Hardin and Lamkin,[1] have found a significant increase in unsteady lift response when the blade has mean loading. The effect found is not based on whether or not the combined unsteadiness and mean lift causes locally transonic conditions. Although corrections to the lift response models should be made if convenient forms become available, it is believed at present that such corrections would be secondary in the HHC/BVI noise problem to the BVI geometry and vortex strength effects.

Conclusions

This study demonstrates how noise directivity, levels, and pressure time histories are significantly modified by the use of HHC. The results support the key conclusion of previous testing that HHC can be used to reduce BVI noise for descending flight conditions where BVI noise is most important. This is particularly significant because of the diversity in rotor types used in the investigations. An interesting feature of the present data is the strong role that rotor aeroelasticity plays in the BVI noise results. This is apparent because similar noise reductions were found here, but with different HHC amplitudes and phases.

A theoretical analysis, using the rotor performance code CAMRAD and a new high resolution version called HIRES, has provided a physical picture of the effect of HHC on aerodynamic and aeroelastic blade behavior, as well as its resultant noise. The low-frequency noise increase is due to the cyclic loading acting over the rotor disk from the use of HHC. Midfrequency BVI noise is increased or decreased by the modifications in the geometry of the BVI, as well as the strengths of the tip vortices. The BVI geometries are determined by the integrated-induced velocities, acting along the vortex path over the rotor disk, in turn determined by the cyclic loading. Comparisons of predictions to acoustic data show that many of the important features of BVI noise and the effect of HHC on this noise are captured by the code HIRES.

The strong influence of global loading found for the results suggest that the idea of using pitch control only in very localized regions where BVI occurs, to reduce BVI noise, would not produce optimum results. Localized pitch control at the BVI would not change the tip vortex strength or its intersection geometry (except with regard to BVI angle of attack). The use of HHC or, better, individual blade control (IBC) to tailor the global loading would appear to be the proper approach. With either control, there is a question as to whether the most desired approach is open-loop (prescribed, as used here) or closed-loop (iterative) control. Although noise prediction technology can eventually play a significant role in defining particular pitch schedules, its use to define a purely open-loop control system would not appear, in the foreseeable future, to provide a desired degree of confidence. A closed-loop control system employing body-mounted microphones should prove to be useful; but, because of uncertainty due to directivity effects, the use of distributed blade mounted pressure or flow devices would be the most reliable in reducing noise in the desired direction.

Acknowledgments

The authors would like to thank R. E. Grandle, Senior Engineer, AcoD, NASA LaRC, for directing the implementation of the advanced data acquisition method used in the test. Also great appreciation is extended to the DLR-FM rotor test team, the DLR-EA acoustic technicians, and the fine DNW staff.

References

[1]Hardin, J. C., and Lamkin, S. L., "Concepts for Reduction of Blade/Vortex Interaction Noise," *Journal of Aircraft*, Vol. 24, No. 2, 1987, pp. 120–125.

[2]Wood, E. R., Powers, R. W., and Hammond, C. E., "On Methods for Application of Harmonic Control," *Vertica*, Vol. 4, No. 1, 1980, pp. 43–60.

[3]Brooks, T. F., and Booth, E. R., Jr., "Rotor Blade-Vortex Interaction Noise Reduction and Vibration Using Higher Harmonic Control," 16th European Rotorcraft Forum, Glasgow, Scotland, UK, Sept. 1990.

[4]Brooks, T. F., and Booth, E. R., Jr., Jolly, J. R., Jr., Yeager, W. T., Jr., and Wilbur, M. L., "Reduction of Blade-Vortex Interaction Noise Through Higher Harmonic Pitch Control," *Journal of the American Helicopter Society*, Vol. 35, No. 1, 1990, pp. 86–91.

[5]Splettstoesser, W. R., Lehman, G., and Van der Wall, B., "Higher Harmonic Control of a Helicopter Rotor to Reduce Blade-Vortex Interaction Noise," *Z. F. W. (Zeitschrift fur Flugwissenschaften)*, Vol. 14, 1990, pp. 109–116; also the 15th European Rotorcraft Forum, Sept. 1989.

[6]Polychroniadis, M., "Generalized Higher Harmonic Control, Ten Years of Aerospatiale Experience," 16th European Rotorcraft Forum, Glasgow, Scotland, UK, Sept. 1990.

[7]Splettstoesser, W. R., Schultz, K.-J., Kube, R., Brooks, T. F., Booth, E. R., Niesl, G., and Streby, O., "BVI Impulsive Noise Reduction by Higher Harmonic Pitch Control: Results of a Scaled

Model Rotor Experiment in the DNW," 17th European Rotorcraft Forum, Berlin, Germany, Sept. 1991.

[8]Lehmann, G., and Kube, R., "Automatic Vibration Reduction at a Four Bladed Hingeless Model Rotor—A Wind Tunnel Demonstration," 14th European Rotorcraft Forum, Milano, Italy, Sept. 1988.

[9]Brooks, T. F., Jolly, J. R., and Marcolini, M. A., "Helicopter Main Rotor Noise—Determination of Source Contributions Using Scaled Model Data," NASA TP-2825, Aug. 1988.

[10]Martin, R. M., Splettstoesser, W. R., Elliot, J. W., and Schultz, K.-J., "Advancing-Side Directivity and Retreating-Sign Interactions of Model Rotor Blade-Vortex Interaction Noise," NASA TP-2784, AVSCOM VR 87-B-3, May 1988.

[11]Brooks, T. F., Booth, E. R., Boyd, D. D., Splettstoesser, W. R., Schultz, K.-J., Kube, R., Niesl, G. H., and Streby, O., "HHC Study in the DNW to Reduce BVI Noise—An Analysis," AHS/RAeS International Technical Specialists Meeting—Rotorcraft Acoustics and Fluid Dynamics, Philadelphia, PA, Oct. 1991.

[12]Johnson, W., "A Comprehensive Analytical Model of Rotorcraft Aerodynamics and Dynamics, Part 1, Analysis and Development," NASA TM-81182, June 1980.

[13]Johnson, W., "Calculation of Blade-Vortex Interaction Airloads on Helicopter Rotors," *Journal of Aircraft*, Vol. 26, No. 5, 1989, pp. 470–475.

[14]Widnall, S., "Helicopter Noise Due to Blade-Vortex Interaction," *Journal of the Acoustical Society of America*, Vol. 50, No. 1, 1971, pp. 354–365.

[15]Richards, E. J., and Mead, D. J., *Noise and Acoustic Fatigue in Aeronautics*, Wiley, London, 1968.

[16]Myers, M. R., and Kerschen, E. J., "Effect of Airfoil Mean Loading on Convected Gust Interaction Noise," AIAA Paper 84-2324, Oct. 1984.

[17]Kerschen, E. J., and Myers, M. R., "Influence of Airfoil Mean Loading on Convected Gust Interaction Noise," *Aero and Hydro-Acoustics, International Union of Theoretical and Applied Mechanics Symposium, Lyon, France, 1985*, Springer-Verlag, Berlin, 1986, pp. 13–20.

[18]Kerschen, E. J., and Myers, M. R., "A Parametric Study of Mean Loading Effects on Airfoil Gust Interaction Noise," AIAA Paper 87-2677, Oct. 1987.